Proceedings of the ASME 2021 International Technical Conference and Exhibition on Packaging and Integration of Electronic and Photonic Microsystems
InterPACK2021
October 26 - 28, 2021, Virtual Conference

InterPACK2021-73270

RACK-LEVEL THERMOSYPHON COOLING AND VAPOR-COMPRESSION DRIVEN HEAT RECOVERY: CONDENSER MODEL

Rehan Khalid
Dept. of Mechanical Engineering
Villanova University
800 Lancaster Avenue
Villanova, PA, USA, 19085
Email: r.khalid@villanova.edu

Raffaele Luca Amalfi
Thermal Management Group
Nokia Bell Laboratories
600-700 Mountain Avenue
Murray Hill, NJ, USA, 07974
Email: raffaele.amalfi@nokia-bell-labs.com

Aaron P. Wemhoff
Dept. of Mechanical Engineering
Villanova University
800 Lancaster Avenue
Villanova, PA, USA, 19085
Email: aaron.wemhoff@villanova.edu

ABSTRACT

This paper is focused on the modeling of a brazed plate heat exchanger (BPHE) for a novel in-rack cooling loop coupled with heat recovery capability for enhanced thermal management of datacenters. In the proposed technology, the BPHE is acting as a condenser, and the model presented in this study can be applied in either the cooling loop or vapor recompression loop. Thus, the primary fluid enters as either superheated (in the vapor recompression loop) or saturated vapor (in the cooling loop), while the secondary fluid enters as a sub-cooled liquid. The model augments an existing technique from the open literature and is applied to condensation of a low-pressure refrigerant R245fa. The model assumes a two-fluid heat exchanger with R245fa and water as the primary and secondary fluids, respectively, flowing in counterflow configuration; however, the model can also handle parallel flow configuration. The 2-D model divides the heat exchanger geometry into a discrete number of slices to analyze heat transfer and pressure drops (including static, momentum and frictional losses) of both fluids, which are used to predict the exit temperature and pressure of both fluids. The model predicts the exchanger duty based on the local energy balance. The predicted values of fluid output properties (secondary fluid temperature and pressure, and primary fluid vapor quality and pressure) along with heat exchanger duty show good agreement when compared against a commercial software.

Keywords: Data centers, Electronics cooling, Liquid-cooling, Mathematical modeling, Modeling, Thermal management of electronics

NOMENCLATURE

Roman	
b	*pressing depth, (m)*
Bo	*Bond number, (–)*
D	*diameter, (m)*
G	*mass flux, ($kg/m^2.s$)*
g	*acceleration due to gravity, (m/s^2)*
h	*enthalpy, (J/kg)*
Hg	*Hagen number, (–)*
k	*thermal conductivity, (W/m/K)*
L	*length, (m)*
l	*slice length, (m)*
N_{pass}	*Number of passes in heat exchanger*
Nu	*Nusselt number, (–)*
p	*pressure, (Pa)*
Pr	*Prandtl number, (–)*
Re	*Reynolds number, (–)*
T	*temperature, (K)*
U	*Overall Heat Transfer Coefficient ($W/m^2.K$)*
u	*velocity, (m/s)*
w	*width, (m)*
x	*Mass-based quality*
We	*Weber number, (–)*

Copyright © 2021 by ASME

Greek

α	*heat transfer coefficient, ($W/m^2.K$)*
β	*chevron angle, (°)*
δ	*plate thickness, (m)*
Δ	*difference, (–)*
Λ	*wavelength of surface corrugation, (m)*
μ	*dynamic viscosity, ($Pa \cdot s$)*
v	*specific volume, (m^3/kg)*
ρ	*density, (kg/m^3)*
σ	*surface tension, (N/m)*

Subscripts

chnl	*channel*
eq	*equivalent*
f	*saturated liquid*
g	*saturated vapor*
h	*Hydraulic*
i	*inlet*
l	*Liquid*
m	*Mean*
o	*outlet*
p	*port*
pri	*primary fluid*
rel	*relative*
sec	*secondary fluid*
v	*vapor*

Acronyms

BPHE	*Brazed Plate Heat Exchanger*
CPU	*Central Processing Unit*
CRAC	*Computer Room Air Conditioning*
CRAH	*Computer Room Air Handling*
EEV	*Electronic Expansion Valve*
EU	*European Union*
HTC	*Heat Transfer Coefficient*
HX	*Heat exchanger*
IT	*Information Technology*
PHE	*Plate Heat Exchanger*
TCO	*Total Cost of Ownership*

1. INTRODUCTION

Thermal management of datacenters is a growing problem dictated by the need of hardware densification for improved computational efficiency and green regulations for deploying eco-friendly solutions. For example, the European Union (EU) has commissioned a set of regulations in 2019 in order to meet the goal of making Europe climate-neutral by 2050 [1].

Approximately, between 25% - 55% of the total energy consumed by most modern datacenters is required to run conventional air-cooling systems. This generates a significant amount of low-grade waste heat, which is of little economic value. Air-cooling systems require fans, blowers, Computer Room Air Conditioning (CRAC) (or Computer Room Air Handling – CRAH) units for the recirculation of cold air across the multiple length scales of a datacenter (server-, rack- and room-levels) in order to keep the temperature of the Central Processing Units (CPUs), and other Information Technology (IT) hardware components, within their maximum allowable values for proper operation [2]. Alternative cooling technologies, such as pumped direct liquid-cooling via cold plate evaporators or active and passive immersion cooling solutions, are beneficial to increase datacenters' heat density, but they may present challenges associated with complexity, Total Cost of Ownership (TCO) and reliability, in addition to broad deployment, covering greenfield and brownfield implementations [3].

This study investigates a similar, yet novel, in-rack thermal management solution for datacenters that incorporates a passive two-phase thermosyphon coupled with a heat pump for simultaneous cooling and heat recovery using mechanical vapor recompression [4]. Refrigerant-based systems are well-known to be thermodynamically more efficient than traditional air-based and liquid-based cooling systems, while lowering the TCO (the latter includes both capital and operating expenses). The suggested working fluids for the proposed system includes high nominal boiling point refrigerants, such as R245fa or R1233zd(E), that lead to lower pressures during datacenter operation.

The focus of this paper is to introduce the novel thermal management system that provides nearly energy-free cooling of a fully populated server rack and production of hot water for heat recovery, followed by a detailed modeling study of BPHEs, which are the key components of the technology. The modeling technique and simulation results are fully discussed, and predictive capabilities are validated against a commercial software.

2. THERMAL MANAGEMENT SYSTEM

The thermal management solution proposed in this study couples in-rack passive two-phase cooling via a thermosyphon loop and a vapor compression cycle for upgrading and reusing the heat captured from the server exhaust. Figures 1 and 2 show the schematic of the flow loop and the experimental apparatus respectively.

In this technology, the evaporator of the thermosyphon is installed inside a sealed rack and is an air-to-refrigerant Heat Exchanger (HX) able to capture the heat from the IT equipment. The refrigerant is then boiled in the evaporator, generating a mixture of liquid and vapor phase, that is guided upward to reach the liquid-vapor separator through the riser tube. The separator tank physically separates the vapor phase from the liquid phase,

Copyright © 2021 by ASME

which is then guided downward to the evaporator through the downcomer tube to repeat the cycle. The use of the separator is important to ensure sufficient liquid head for stable cooling operation, as well as to reduce sub-cooling at the inlet of the evaporator for fast start-up operation. On the other hand, the heat pump cycle operates using traditional vapor-compression cycle components, including a compressor, BPHE condenser, BPHE regenerator and an expansion valve, where the saturated two-phase mixture reaches the liquid-vapor separator completing the cycle.

Figure 1 shows two BPHEs in the proposed thermal management and heat recovery solution, namely the regenerator and the condenser. Figure 2 shows the assembled system prototype that is depicted by the schematic of Figure 1. Two BPHE condensers can be easily seen in this picture, labeled LP Condenser and HP Condenser, and stand for Low-Pressure and High-Pressure Condenser, respectively. The LP Condenser is located in the cooling loop and the HP condenser is located in the heat recovery (vapor recompression) loop, and are labeled so to indicate the relative pressure of the refrigerant that they receive. The regenerator can be spotted in the upper right of the HP Condenser.

The LP Condenser acts as the sink for the cooling loop, receiving low-pressure vapor directly from the LV separator. The HP Condenser acts as the sink for the heat recovery loop, and receives high-pressure vapor from the compressor, which itself receives vapor form the LV separator through the regenerator. Finally, it is noteworthy that the object labeled Condenser in Figure 1 corresponds to the HP Condenser in Figure 2, while the LP condenser is not shown in Figure 1.

These BPHEs play a vital role in the overall architecture of the proposed thermal management solution. Thus, they need to be properly designed to be able to improve thermosyphon thermal-hydraulic performance and reduce compressor input power. An introduction to plate heat exchangers (PHEs) and the associated modeling technique is reported in the next section.

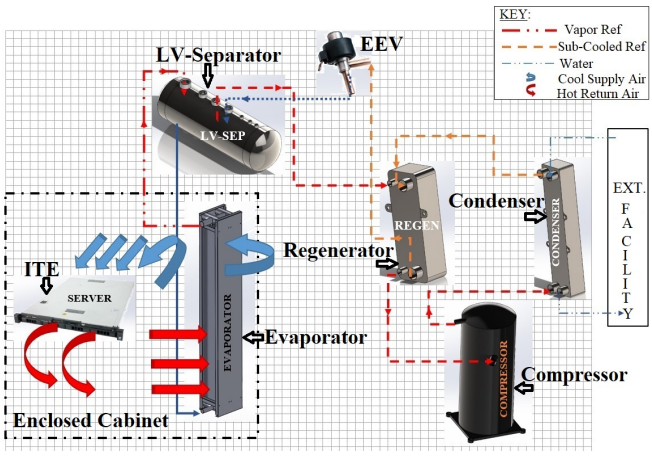

Figure 1: SCHEMATIC OF THE PROPOSED THERMAL MANAGEMENT AND HEAT RECOVERY SYSTEM.

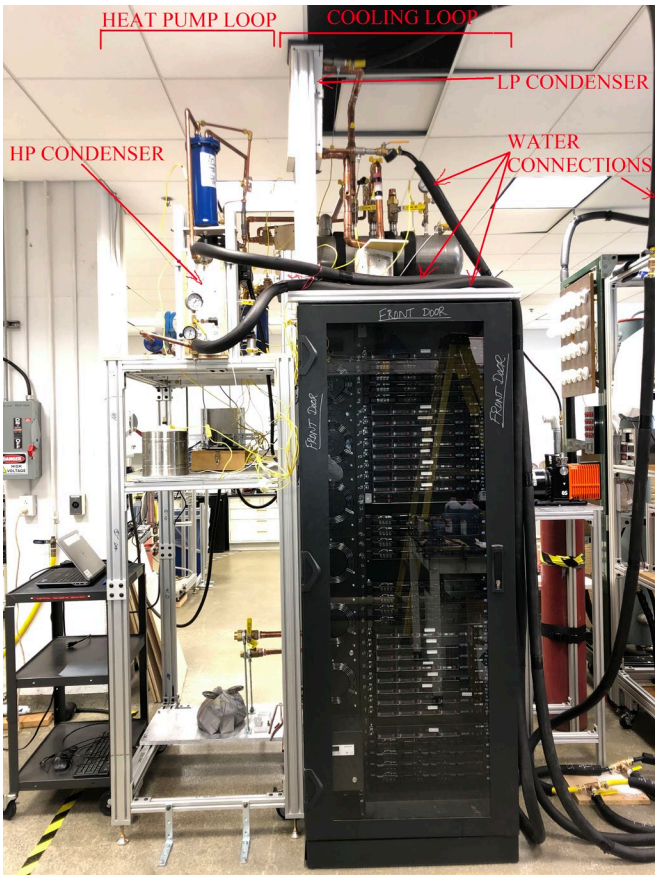

Figure 2: EXPERIMENTAL APPARATUS ASSEMBLED AT VILLANOVA UNIVERSITY.

3. PLATE HEAT EXCHANGER MODELING

PHEs comprise rectangular corrugated plates that are stacked together to create alternating flow passages for the primary and secondary fluids. The plates are stamped from thin metal sheets, commonly made of stainless steel, to minimize conductive thermal resistance and are obtained with corrugated patterns that enhance local heat transfer performance.

PHEs have increasingly become the preferred solution in many industrial applications due to their flexibility in accommodating different heat loads by adding or removing plates, as well as by changing the plate geometry. Furthermore, depending on the application, several types of PHEs are available, including gasketed, welded, semi-welded, brazed and shell-and-plate heat exchangers. However, the authors have selected BPHEs because of their high efficiency, reduced form factor and long service lifetime. Figure 3(a) provides an example of a BPHE, while Figure 3(b) shows a schematic of the chevron plate geometry.

Copyright © 2021 by ASME

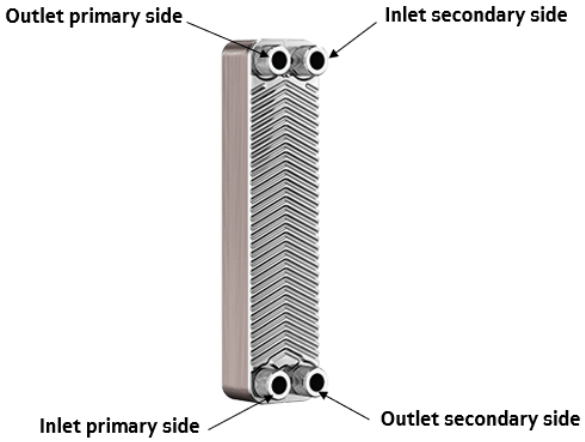

(a)

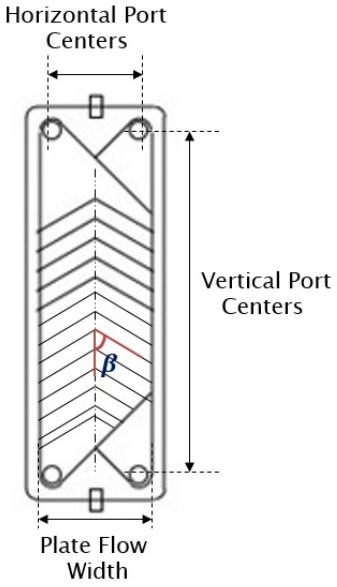

(b)

Figure 3: a) PHOTOGRAPH OF A BPHE THAT OPERATES IN COUNTER-FLOW ARRANGEMENT; (b) SCHEMATIC OF A SINGLE CHEVRON PLATE WITH THE CORRESPONDING GEOMETRICAL PARAMETERS.

A general modeling technique for accurate designs of BPHEs operating in two-phase-to-single-phase flow (e.g., low or high-pressure condenser in Figure 2), as well as for single-phase-to-single-phase flow (e.g., regenerator in Figure 1) is presented in the current study.

4. MODEL COMPARISON

The model presented in this study augments the technique introduced by Qiao et. al [5]. The core model, which consists of the Slice Solver, remains the same between the current implementation and that introduced in [5]. However, three key differences separate the two approaches, as detailed below.

The current model assumes a two-fluid HX, where the flow configuration is either parallel-flow or counter-flow, and the number of passes / junctions executed by each fluid, as it flows through the plates, is only one (i.e., the HX is single-pass for both fluids). The counter-flow configuration is treated as parallel-flow but with a reversal in heat transfer direction [6], as will be explained later. The technique presented by Qiao et al. [5], however, is general in nature and is able to handle multiple passes, more than two fluids and complex configurations by adopting the Junction-Channel Connectivity Matrix approach mentioned in the same study.

Another key difference includes the omission of the Top-Level solver in the current model, whereby the entire HX geometry is solved sequentially as opposed to iteratively with the same state (pressure and enthalpy) in each iteration [5]. This speeds up the simulation as compared to the iterative process adopted in [5], unless the individual slices are solved in parallel using parallel computing techniques.

Lastly, the model in this study assumes that the primary fluid can change phase, while the secondary fluid does not change phase and is maintained in single-phase flow. Since the model is representative of a condenser, it is expected that the primary fluid (hot side) enters as either superheated or saturated vapor, undergoes a condensation heat transfer process and exits as either a two-phase mixture with a very low quality (including saturated liquid) or as a sub-cooled liquid. Conversely, the secondary fluid (cold side) is expected to enter as a sub-cooled liquid and exit as such but at a higher temperature and lower-pressure due to the sensible heat transfer process.

The current model thus focuses on accurately modeling the condensation process and can identify four regimes for the primary fluid: i) superheated vapor flow, ii) superheated vapor condensing flow, iii) saturated two-phase condensing, and iv) sub-cooled liquid flow. The first and last regimes are representative of pure single-phase cooling, while the second and third regime represent a phase-change process. The inclusion of the 'superheated vapor condensing' regime captures the physics of the condensation process more accurately by identifying that the actual condensation process begins at a cut-off relative enthalpy [7] greater than the relative enthalpy corresponding to that of saturated vapor (when the vapor quality is equal to 1.0).

The concept of relative enthalpy extends the definition of the static (mass-based) fluid quality beyond the confines of the two-phase region, where the vapor quality is restricted between 0 and 1, i.e. between saturated liquid and saturated vapor enthalpy. The relative enthalpy is determined in exactly the same manner as the fluid static quality within the two-phase region, with the only difference being that now the fluid enthalpy is not bounded by the two saturated state enthalpies.

$$x_{rel} = \frac{h - h_f}{h_g - h_f} \tag{1}$$

It should be pointed that although models for condensers have been successfully validated and published by Eldeeb et. al [8], their work is an extension of [5]. Even though the current

Copyright © 2021 by ASME

study approaches the same phenomenon of condensation heat transfer, it is done so with the key differences mentioned above.

Finally, emphasis is placed on the use of suitable and accurate correlations for predicting the heat transfer coefficient (HTC) and friction factor for various regimes of the two fluids, as will be detailed in the next section.

5. MODEL DEVELOPMENT

The number of active plates in a BPHE are those that are directly involved in the heat exchange between the two fluids, contributing to the overall effective heat transfer area. The number of active plates can be determined based on either the total number of plates or the total number of channels. The wall temperatures of these plates plays a vital role in the heat transfer process. For each active plate, two wall temperatures can be determined, based on either face [Left (L) or Right (R)] of the plate. A simplified schematic of the condenser considered in this study is shown in Figure 4.

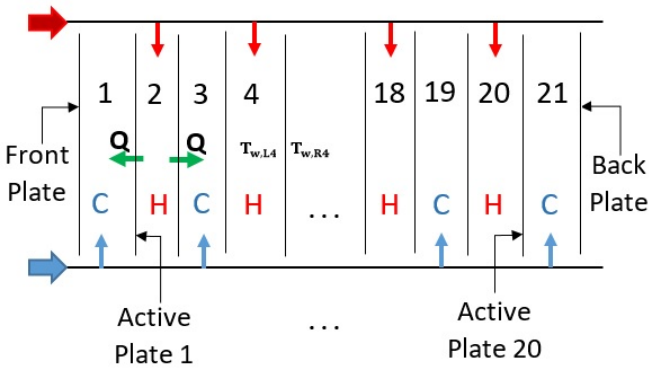

Figure 4: NUMBER OF CHANNELS, ACTIVE PLATES AND FLUID FLOW REPRESENTATION IN A BPHE CONDENSER.

The schematic reported in Figure 4 shows the condenser divided into individual channels for the hot and cold fluid, as well as the type and direction of fluid in each channel. The channels are numbered from 1 to 21, while the 'C' and 'H' designation stands for hot and cold fluid. The schematic shows that the BPHE comprises a total of twenty-two plates, including the two end plates that hold the remaining (active) plates together and are considered adiabatic. The twenty-two plates yield twenty-one channels for the fluid flow and a total of twenty active plates.

As mentioned previously, the model divides the condenser into an 'M x N' grid, where 'M' denotes the number of slices of equal width that the BPHE is divided into, while 'N' denotes the total number of channels that the plate HX comprises of. Nodes are placed at the exit of each slice, and the fluid state at each node is determined based on the computed temperature and pressure value at those points. A representative grid based on N channels is shown in Figure 5 (N is odd for this case), where the schematic has been simplified compared to Figure 4 to focus on representation of the nodes, slices and segments that the BPHE is divided into. It is noteworthy that a single slice encompasses each horizontal rectangle only, but is shown enlarged in order to account for the thickness of the nodes drawn (i.e., the nodes are part of the slice indicated in Figure 5). In reality, the nodes exist only at the boundaries and do not cross into the adjacent slices.

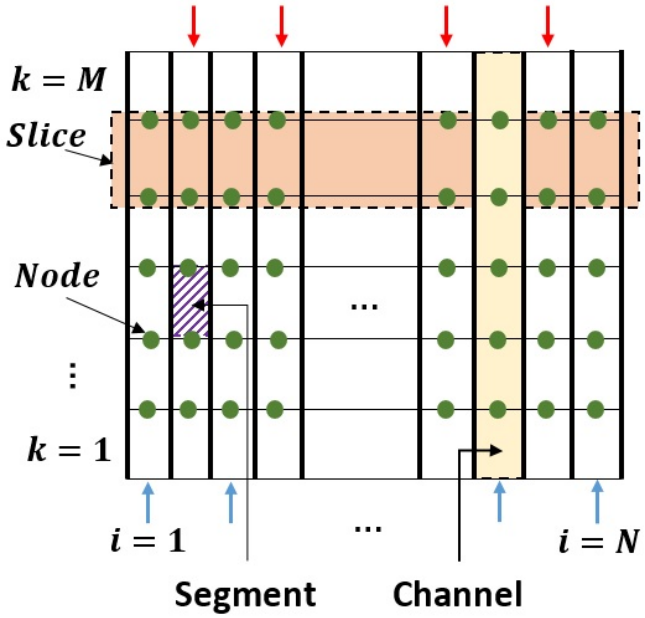

Figure 5: BPHE DIVIDED INTO A GRID PATTERN.

The model proposed by the authors in [5] has been developed under the following key assumptions:

- All transport properties are evaluated based on segment inlet conditions and plate temperatures on both sides are constant within a segment;
- Heat transfer coefficients are determined based on segment inlet properties and are constant within a segment;
- Phase-change only occurs at the segment boundaries (called nodes as shown in Figure 5), meaning that the model will not further subdivide a segment into further segments;
- The overall heat exchanger and end plates are assumed to be adiabatic (i.e. no heat loss due to natural convection) with negligible longitudinal heat conduction along the plate;
- Heat conduction along the fluid flow path is not considered, while heat conduction across the walls within a given segment is included;
- Viscous heating through the inlet and outlet tubes and manifolds is neglected. Hence, the temperature and enthalpy of each fluid upon entering the channels is the same as that of the fluid entering the HX;
- The pressure drop through the inlet and outlet tubes is neglected, so only the pressure drop through the ports is considered.

Based on the above specified assumptions, a mathematical model for the heat transfer and pressure drop inside the heat exchanger is developed, as initially presented in [5]. The model

Copyright © 2021 by ASME

first determines which fluid should flow in each channel based on the total number of channels and the number of channels for each fluid. More specifically, for a BPHE with an even number of total channels, the number of channels attributed to both types of fluid are the same, and the choice of fluid for the first channel is arbitrary (i.e. either fluid can flow in the first channel and subsequent channels will alternate the fluids). However, for a BPHE with an odd number of channels, one fluid will flow in more channels than the other with a difference of one channel. Each fluid's incoming enthalpy is also determined based on a combination of two out of three possible state variables: the incoming temperature, pressure and quality. The pressure drop through a single port is subsequently determined based on the homogenous flow model, as given by [9]:

$$\Delta P_{port} = 0.75\left(\frac{u_m^2}{2v_m}\right) \tag{2}$$

Where u_m is the mean fluid velocity through the port, calculated from the fluid mass flux based on the inner diameter of the port, G_{port}, and mean specific volume of the fluid, v_m, as follows:

$$u_m = G_{port} v_m \tag{3}$$

Inserting Eq. (3) into (2) and accounting for multiple passes yields

$$\Delta P_{port} = 0.75\left[\left(\frac{G_{port}^2}{2\rho_f}\right)_i + \left(\frac{G_{port}^2}{2\rho_m}\right)_o\right] N_{pass} \tag{4}$$

Where N_{pass} equals one for the given HX, ρ_i is the fluid density at the entrance of the inlet port (assuming single-phase), and ρ_m is the mean fluid density at the inlet of the exit port (assuming a two-phase mixture). The mean density is evaluated based on the mean vapor quality, x_m, as

$$\rho_m = \left[(1 - x_m)v_f + x_m v_g\right]^{-1} \tag{5}$$

$$x_m = 0.5(x_i + x_o) \tag{6}$$

The pressure drop through the inlet port should be evaluated at the beginning of the simulation before evaluating the first slice, using stream inlet conditions to the HX. Similarly, the outlet port pressure drop should be evaluated after solving all the slices, using average stream conditions exiting the HX. The fluid density entering the outlet port should be evaluated using these averaged conditions. Finally, Equation (4) represents the sum of the inlet and outlet port pressure drop for a given fluid stream.

The 'Slice Solver' [5] is then called to solve the governing equations in all the slices in order to determine the state at all nodes. For a fluid in single-phase flow, the nodal temperature and pressure is first determined and then subsequently used to determine the nodal enthalpies. For a two-phase fluid, however, the nodal pressure and enthalpy (using energy balance) are first determined, and these properties are then used to calculate the nodal temperature. The outlet nodes for one slice subsequently become the input for the next slice, and its output state is then determined using the Slice Solver. In this manner, all the slices are sequentially solved until the last slice is reached. The last slice is solved in the same manner as the previous slices (fictitious nodes present at the outlet of the last slice). The enthalpy at the fictitious nodes of the last slice is then averaged to determine a single value of fluid enthalpy. The pressure is also averaged after accounting for the outlet port pressure drop. The averaged pressure and enthalpy are used to determine the fluid temperature leaving the HX. Hence, each fluid stream's outlet state can be determined for a given set of inlet conditions and HX geometry.

Lastly, since the model is based on a fixed-boundary method, the number of slices are not further sub-divided to track the location of the interface between the two-phases. The number of slices, *M*, should be pre-determined so as to cause the phase-change process as near to a slice boundary as possible. This is done through hit-and-trial before the actual simulation, but reduces the actual simulation time since additional computational resources are not allocated to determining the liquid-vapor interface. Once a satisfactory base value of the number of slices has been determined, the vertical grid size i.e. *M* can be altered in multiples of *M* until grid independence is achieved.

a) GOVERNING EQUATIONS

The variables to be solved in the slice solver are the wall temperatures of the active plates. In particular, for a HX with *N* active plates (*N+2* plates in total), there are *2N* wall temperatures. Thus, *2N* equations are needed to solved for the same number of variables. This gives a system of equations that can then be solved to yield the wall temperatures. Once the wall temperatures are known, it is possible to determine either the nodal temperature at the outlet of a given slice for a fluid in single-phase flow or the nodal enthalpy for a fluid undergoing two-phase flow. The fluid pressure drop across the segment is calculated independently of the wall temperatures using the static, momentum and frictional components of the pressure drop. The development of the equations for the wall temperatures for single-phase and two-phase are described below.

i. Single-Phase Flow

Consider a single segment (per Figure 5) located in a hot fluid channel in the middle of the HX (other than first or last channel), as shown in Figure 6 below.

Copyright © 2021 by ASME

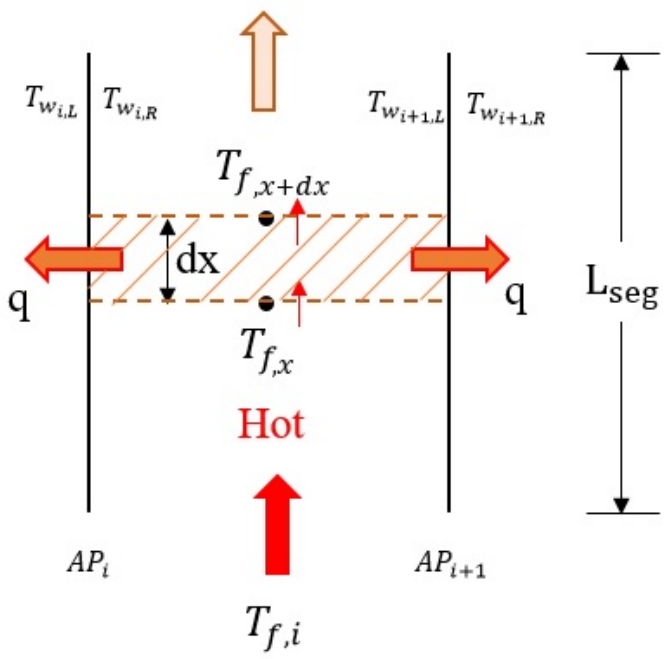

Figure 6: DETAILS OF A SINGLE SEGMENT.

Applying an energy balance to the differential segment of width dx gives the following:

$$\dot{E}_{in} - \dot{E}_{out} = 0$$

$$\rightarrow \dot{m}c_p T_{f_x} - \left[\dot{m}c_p T_{f_{x+dx}} + \alpha(dx.y)\left(T_f - T_{w_{i,R}}\right) + \alpha(dx.y)\left(T_f - T_{w_{i,R}}\right)\right] = 0 \quad (7)$$

where y is the width of the segment into the page, equal to the width of the plate, and is given by

$$y = w \equiv \frac{A_{seg}}{L_{seg}} \quad (8)$$

Applying a Taylor Series expansion on the term $\dot{m}c_p T_{f_{x+dx}}$ gives

$$\dot{m}c_p T_{f_{x+dx}} = \dot{m}c_p T_{f_x} + \dot{m}c_p \frac{dT_{f_x}}{dx} dx \quad (9)$$

Substituting Eqs. (8) - (9) into Eq. (7) and simplifying yields

$$\frac{dT_{f_x}}{dx} = -\left(\frac{\alpha A_{seg}}{\dot{m}c_p L_{seg}}\right)\left(T_f - T_{w_{i,R}}\right) - \left(\frac{\alpha A_{seg}}{\dot{m}c_p L_{seg}}\right)\left(T_f - T_{w_{i+1,L}}\right) \quad (10)$$

Equation (10) can then be cast into the form of a standard ordinary differential equation (ODE) and solved for $T_f(x)$, which is the temperature distribution of a single-phase fluid within the segment for a middle channel:

$$T_f(x) = 0.5\left(T_{w_{i,R}} + T_{w_{i+1,L}}\right) + \left[T_{f_i} - 0.5\left(T_{w_{i,R}} + T_{w_{i+1,L}}\right)\right] e^{-\left(\frac{2\alpha A_{seg}}{\dot{m}c_p L_{seg}}\right)x} \quad (11)$$

A similar analysis ensues for the two end channels, with the heat transfer only considered in one direction (towards the middle of the HX) since the two end plates are assumed to be adiabatic. This approach yields the following temperature distributions for the first and last channels of the HX, as given by Eqs. (12) and (13) respectively:

$$T_f(x) = T_{w_{i+1,L}} + \left[T_{f_i} - T_{w_{i+1,L}}\right] e^{-\left(\frac{\alpha A_{seg}}{\dot{m}c_p L_{seg}}\right)x} \quad (12)$$

$$T_f(x) = T_{w_{i,R}} + \left[T_{f_i} - T_{w_{i,R}}\right] e^{-\left(\frac{\alpha A_{seg}}{\dot{m}c_p L_{seg}}\right)x} \quad (13)$$

The fluid temperature at the segment outlet can then be determined by setting $x = L_{seg}$, which is the temperature at the outlet node of the given slice.

It has to be noted that Eqs. (11) – (13) are similar, and can be cast into a general form as

$$T_f(x) = \Gamma + \left[T_{f_i} - \Gamma\right] e^{-\zeta x} \quad (14)$$

The term Γ is only a function of the two wall temperatures on the inside faces of the plates that make up a given channel, while the parameter ζ is primarily dependent on the fluid properties and the rate of heat advection to the adjacent channels, captured using the heat transfer coefficient, h. A pattern thus exists in the single-phase fluid temperature distribution within each channel for a given slice and the general form makes it convenient to program with a computer.

The fluid properties can be determined based on the state at the inlet nodes for a given slice, which is always known, since the slices are thin and solved sequentially starting with the pre-determined fluid state at the inlet of the channels. The wall temperatures, captured via Γ, are still unknown and can be determined via an energy balance on the channel walls itself.

Consider the 'Hot' channel of Figure 6 but including the next two channels for completeness, as shown in Figure 7.

Copyright © 2021 by ASME

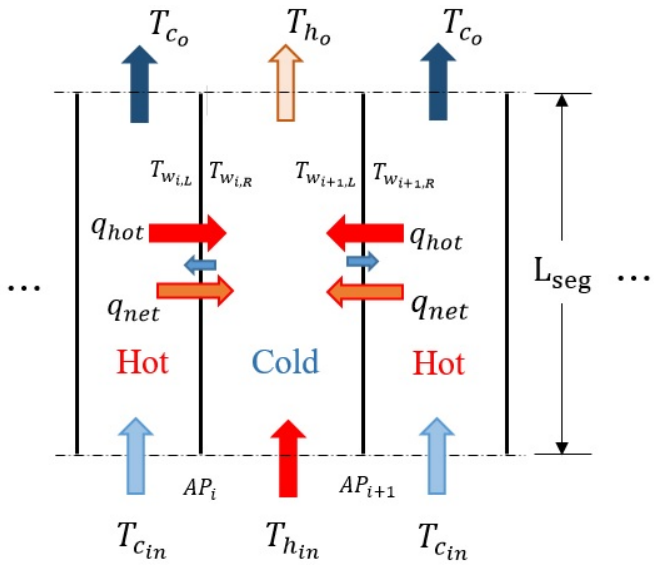

Figure 7: SCHEMATIC TO APPLY WALL ENERGY BALANCE.

An energy balance can be written for active plate AP_i based on the heat exchange between the hot and cold fluid flowing in channels adjacent to the plate. Thus,

$$\dot{Q}_L - \dot{Q}_R = 0 \tag{15}$$

$$\int_0^L d\dot{Q}_L - \int_0^L d\dot{Q}_R = 0 \tag{16}$$

Applying Newton's law of cooling yields:

$$\frac{\alpha_1 A}{L}\int_0^L (T_{h_{in}} - T_{w_{i,L}})dx - \frac{\alpha_2 A}{L}\int_0^L (T_{w_{i,R}} - T_{c_{in}})dx = 0 \tag{17}$$

Finally, substituting the appropriate form of the single-phase fluid temperature distribution (depending on the channel location, one of Eqs. (11) – (13)) and re-arranging yields an equation involving the plate temperatures as a function of the fluid properties, HTCs and the fluid temperature at the inlet of the channel.

Further, a surface energy balance on the left face of plate AP_i (i.e., going from hot fluid into the plate) gives

$$\dot{Q}_L - \dot{Q}_{cond} = 0 \tag{18}$$

Applying Newton's law of cooling and Fourier's law of heat conduction to the respective terms yields

$$\frac{\alpha_1 A}{L}\int_0^L \left(T_{h_{in}} - T_{w_{i,L}}\right)dx - \left(\frac{T_{w_{i,L}} - T_{w_{i,R}}}{\delta}\right) k_{pl} A = 0 \tag{19}$$

Again, substituting the appropriate form of the single-phase fluid temperature distribution and re-arranging yields a second equation for the wall temperatures. The same process can be repeated for active plate AP_{i+1}, where the residual equations would read as follows, owing to the reversal in direction of net heat flow:

$$\dot{Q}_R - \dot{Q}_L = 0 \tag{20}$$

$$\dot{Q}_{cond} - \dot{Q}_L = 0 \tag{21}$$

The same procedure can be repeated for subsequent active plates (starting initially from the first active plate), thereby yielding 2N equations in 2N variables (for the 2N plates). The equation set can then be solved using an appropriate numerical scheme, such as the Gauss-Seidel method, to yield the single-phase fluid temperature at the outlet of the slice.

Equations (15) and (18) represent the residual equations for the active plates with the hot fluid to the left of the plate, while Equations (20)-(21) represent for plates with a hot fluid to its right. Similar to the temperature distribution case, a pattern emerges in the equation set for odd numbered active plates and even numbered active plates. This allows the equations to be readily programmed and solved using a computer.

The pressure drop across each segment is determined as the sum of friction, momentum and static pressure drops, regardless of the flow phase. For single–phase, since the slices are thin, the density is not expected to change much across a segment; hence, the momentum component of pressure drop is negligibly small and is ignored in the current analysis.

The static pressure change is computed as per Eq. (22), where flow against gravity represents a pressure drop while gravity aided flow (downwards) represents a static pressure rise.

$$\Delta P_{static} = \rho_m g L_{seg} \tag{22}$$

The friction pressure drop is computed using the Moody (Darcy) friction factor, calculated from appropriate correlations found in the literature. These are identified in the next section. The friction pressure drop can then be computed as per Equation (23), where G_{chnl} is the individual fluid mass flux based on the channel mass flow rate and channel hydraulic diameter.

$$\Delta P_{fric} = \frac{2 f L_{seg} G_{chnl}^2}{D_h \rho_m} \tag{23}$$

ii. Two-Phase Flow

For a fluid undergoing phase-change between vapor and liquid (or vice versa), the temperature is a strong function of the pressure [5], being in saturated condition, and hence cannot be used as an independent variable. The analysis thus relies on the fluid mixture's pressure and enthalpy as the two independent variables required to fix its state. These two properties are then used to determine the fluid temperature at the nodes on the slice outlet.

For two-phase flow, the same analysis can be applied to determine the wall temperatures as presented for single-phase flow. However, since the fluid temperature distribution across a segment is unknown, and the slices are thin, it can be argued that there will be minimal variation in the fluid temperature across a segment. Thus, to avoid mathematical complexity in the

Copyright © 2021 by ASME

resulting analysis, a linear variation in the fluid temperature across the segment is assumed [5], as given by

$$T_f(x) = T_{f_i} + \left(\frac{T_{f_o} - T_{f_i}}{L}\right) x \tag{24}$$

This temperature distribution can then be plugged into either of the residual equation sets (Equations (15) and (18) or Equations (20) and (21)), as done before for single-phase flow. The resulting equations will again display a pattern for the odd and even numbered active plates, whereby they can be easily implemented in a computer program, which helps if the HX under analysis has a large number of plates (and by extension, a large number of active plates).

It has to be mentioned that assuming a constant temperature profile (i.e., no variation in temperature across a segment) will oversimplify the analysis and the resulting equations will not yield accurate results. Also note that Eq. (24) features the outlet temperature of the fluid, which is unknown. Thus, the resulting equations have to be solved iteratively with an assumed value of the segment outlet temperature till convergence is reached. This represents another layer of iteration at the segment level (only if phase-change is involved, however), in addition to the iterations at the slice level to converge on the assumed value of the wall temperatures. The solution strategy for the condenser solver is outlined in the flowchart of Figure 8.

The momentum (deceleration) and static pressure change for condensing two-phase flow is determined based on the void fraction as given by

$$\Delta P_{acc} = G_{chnl}^2 \left[\frac{(1-x)^2}{\rho_f(1-\gamma)} + \frac{x^2}{\rho_g \gamma^2}\right] \tag{24}$$

$$\Delta P_{static} = \gamma_m \rho_g + (1-\gamma_m)\rho_f g L_{seg} \tag{25}$$

Where γ_m is the mean void fraction across the segment, determined using Zivi's model [10] as per Eq. (26). The mean void fraction is itself based on the mean quality, as defined by Equation (6).

$$\gamma_m = \left[1 + \left(\frac{1-x_m}{x_m}\right)\left(\frac{\rho_g}{\rho_f}\right)^{2/3}\right]^{-1} \tag{26}$$

The deceleration actually yields a pressure rise since the fluid slows down as more vapor condenses into liquid. Equation (24) is applied in two parts, first using the quality and void fraction at the segment inlet, then doing the same using segment outlet values, and finally taking their difference.

The friction pressure drop is computed as in the single-phase case using friction factors developed for two-phase flow. Correlations for these are specified in the next section.

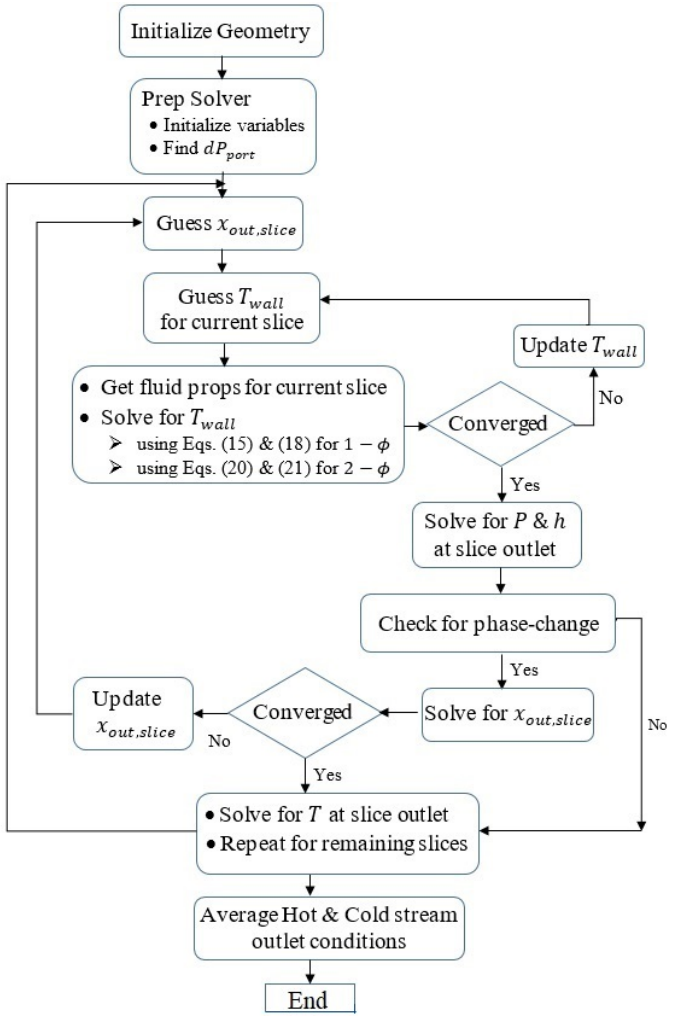

Figure 8: CONDENSER SOLVER FLOWCHART.

b) CORRELATIONS USED

Correlations for the HTC and friction factor for both single and two-phase flow are taken from the literature. For single-phase flow, the HTC and friction factors are determined based on the correlation suggested by Kumar [11], which has been demonstrated reliable results [12]. For two-phase flow, the condensation HTC is determined based on Yan's correlation for R-134a [13], which can predict the performance of R-245fa to within 12% [14]. The use of Yan's correlation is justified by Farzad et. al [15].

Lastly, the two-phase friction factor is based on the correlation developed by Huang et. al [16], who correlate the Fanning friction factor for two-phase flow. This must be converted to the Darcy friction factor before use with Eq. (23).

It is noteworthy that the Huang et al. model has been obtained for flow boiling and not for condensing flow. However, its use is justified by the work of Farzad and Amalfi [15], who explain the correlation in addition to validating the model using both flow boiling and condensation data.

Copyright © 2021 by ASME

c) COUNTER-FLOW CONFIGURATION

In this manner, fluid flow across a BPHE in counter-flow configuration is treated as a pseudo parallel-flow configuration, to keep the solver core strategy the same, regardless of flow configuration. To solve a counter-flow case requires another layer of iteration over the parallel-flow solver, where the hot fluid remains the same but the cold fluid is assumed as a 'less-hot' fluid, thereby flowing in parallel to the hot fluid while 'cooling down' from an initial higher temperature to the required lower temperature specified by the inlet stream.

A simple switch in sign of the fluid temperature distribution of Eq. (14) accounts for the change in heat transfer, since the cold (less-hot) fluid is also 'losing' heat to the hot fluid, while always remaining in single-phase. A general form of Eq. (14) can thus be specified:

$$T_f(x) = \Gamma + (-1)^m \left[T_{f_i} - \Gamma\right] e^{-(-1)^m \beta x} \qquad (27)$$

where the term $(-1)^m$ takes care of the change in direction (sign) of the heat transfer. The exponent m is a binary number and can take on the following values:

$$m = 0 \rightarrow parallel\ flow \qquad (28)$$

$$m = 1 \rightarrow counter\ flow$$

The first guess is based on the mean inlet temperatures of the two fluids, while the second guess is based on an increment of the first guess $(1 \pm \delta)$ where the appropriate sign is based on the sign of the error from the first guess. Subsequent guess values are calculated using the secant algorithm, which ensures stability and rapid convergence of the solution.

The same strategy is implemented for the cold side pressure change, to ensure complete accuracy of the suggested counter-flow scheme (although this may not be required in the strictest sense). Thus, an inlet pressure value, less than the actual specified inlet value for the cold fluid is guessed, in addition to the initial guess for the temperature. From thereon, the $(-1)^m$ term is added when summing the contributions of the different pressure changes, as given by

$$P_{out} = P_{in} + (-1)^m \Delta P_f + (-1)^m \Delta P_s + (-1)^m \Delta P_m \qquad (29)$$

The intention is that any component that was previously contributed to a pressure drop now yields a pressure rise and vice versa, so that the cold fluid has a 'net gain' in pressure from the lower initial guess to the actual higher inlet pressure. The convergence takes place in the same loop as the temperature.

6. MODEL VALIDATION

Prior to validating the model, a grid resolution study is performed. This is essential in balancing model accuracy with computational cost. The number of segments is varied between 1 and 50, where an arbitrary number of segments can be chosen since no phase-change occurs; hence, there is no need to pre-determine a base number of slices, as explained in the last paragraph of section 5, *Model Development*. The resulting HX duty trend versus the number of slices, M, is shown in Figure 9 below. In particular, $M = 30$ slices are selected for further single-phase model validation based on the trend identified in the figure.

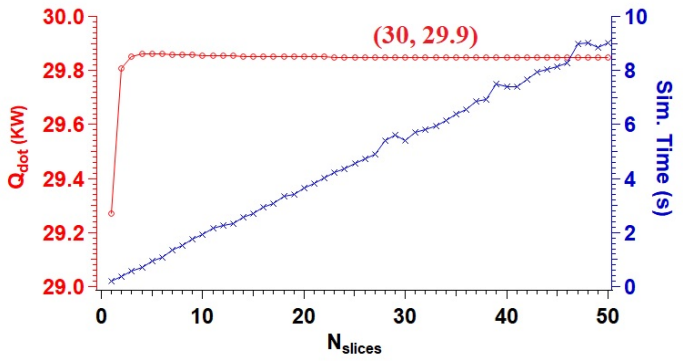

Figure 9: CONDENSER MODEL GRID INDEPENDENCE STUDY FOR SINGLE-PHASE PARALLEL FLOW.

The model is validated against a commercial software, Aspen EDR, for both single-phase liquid flow and two-phase condensation under each flow configuration. The geometry for APV's Junior Plates, which is pre-defined in Aspen EDR, is used for the validation case studies. The model is run with $M = 30$ slices for both the single-phase parallel and counterflow configurations, based on the results of the grid resolution study.

Inlet stream conditions for single-phase water-water heat exchange are specified in Table 1, while outlet stream results are reported in Table 2. In addition, the primary side flows upwards (against gravity) in the single-phase case while it flows downwards (with gravity) for the two-phase case, in order to aid the condensation process. The secondary side, however, switches direction if the flow configuration is counter-flow.

Results show that the heat exchanger duty predicted by the model compares to within 7% and 5% of that predicted by Aspen EDR for the parallel and counter-flow configuration, respectively.

Table 1: BPHE INLET STREAM CONDITIONS FOR WATER-WATER LIQUID FLOW.

Parameter	Primary	Secondary
T_{in} (°C)	80.0	20.0
P_{in} (kPa)	200	200
$\dot{m}$ (kg/h)	1080	720

Copyright © 2021 by ASME

Table 2: BPHE OUTLET STREAM CONDITIONS FOR WATER-WATER IN PARALLEL-FLOW.

Stream Parameter	Primary		Secondary	
	Model	EDR	Model	EDR
T_{out} (°C)	56.3	56.4	55.7	55.5
P_{out} (kPa)	190	182	193	192
$U_{stream,mean}$ (W/m^2.K)	11,100	13,600	7600	8600

Overall Parameter	Model	EDR
$\dot{Q}_{HX}$ (kW)	29.9	32.1
Sim. Time (s)	5.5	9.0

Table 3: BPHE OUTLET STREAM CONDITIONS FOR WATER-WATER IN COUNTER-FLOW.

Stream Parameter	Primary		Secondary	
	Model	EDR	Model	EDR
T_{out} (°C)	48.0	48.2	67.4	67.8
P_{out} (kPa)	190	182	195	192
$U_{stream,mean}$ (W/m^2.K)	11,700	13,900	7500	8500

Overall Parameter	Model	EDR
$\dot{Q}_{HX}$ (kW)	41.2	43.3
Sim. Time (s)	23.2	10.0

Lastly, a case study with R-245fa in condensing flow versus liquid water is performed using the parallel-flow configuration. A grid resolution study is also performed for this case, in order to determine the minimum number of slices needed to balance simulation accuracy with computational cost. In this case, a base number of slices, equal to 28, is selected based on initial hit and trial. This ensured that phase change at the saturated liquid state (x = 0) was achieved as close to a slice boundary as possible, thereby ensuring accuracy of the simulation. With 28 slices, a quality of 1.5% (0.015) was achieved for the middle channels at the outlet of the fourth slice. The resulting grid resolution study, along with the computational cost i.e. simulation time, is shown in Figure 10 below. Based on the figure's left-axis scale, even 84 slices could have been chosen without compromising accuracy; however, $M = 364$ slices were chosen to minimize even the smaller perturbations in the output results and to obtain a close match to the Aspen EDR results.

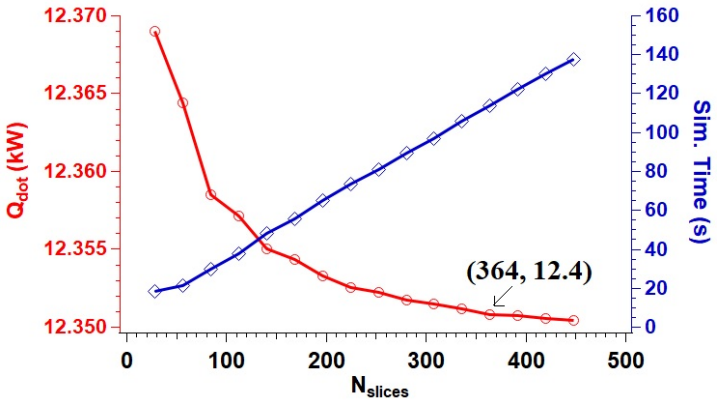

Figure 10: CONDENSER MODEL GRID INDEPENDENCE STUDY FOR TWO-PHASE PARALLEL FLOW.

The stream conditions for this case are presented in Table 4 below, where the R245fa enters as saturated vapor and condenses downwards to the outlet conditions reported in Table 5. Stream output data for the secondary (water) side along with heat exchanger level parameters are also reported in Table 5.

Table 4: BPHE INLET STREAM CONDITIONS FOR R245fa CONDENSATION WITH WATER IN LIQUID FLOW.

Parameter	Primary	Secondary
T_{in} (°C)	85.0	20.0
P_{in} (kPa)	892 (sat. vapor)	200
$\dot{m}$ (kg/h)	200	800

Table 5: BPHE OUTLET STREAM CONDITIONS FOR R245fa AGAINST WATER IN PARALLEL FLOW.

Stream Parameter	Primary		Secondary	
	Model	EDR	Model	EDR
T_{out} (°C)	33.6	33.6	33.3	32.4
P_{out} (kPa)	891	889	201	190
$U_{stream,mean}$ (W/m^2.K)	1160	920	7100	7800

Overall Parameter	Model	EDR
$\dot{Q}_{HX}$ (kW)	12.4	12.5
Sim. Time (s)	115	10.0

The results of Table 5 show that the heat exchanger duty predicted by the model is within 1% of the value predicted by

Copyright © 2021 by ASME

Aspen EDR, thereby showing excellent agreement. In addition, the stream outlet temperatures exhibit a near perfect match.

The interesting thing to note is the pressure drop of the secondary fluid. The model actually predicts a slight increase in the pressure (≈1 kPa) of the secondary fluid, since it flows downwards, aided by gravity. Hence, the static pressure rise slightly offsets the pressure drop caused by friction (momentum pressure drop is negligible for single-phase flow and hence does not contribute).

There is also a slight mismatch in the inlet saturation temperature corresponding to the specified inlet pressure calculated by Aspen (85.3°C versus 85°C specified for the model) for saturated vapor at 892.53 kPa. Given the above discrepancy, the pressure drop predicted for the hot fluid is not surprising, considering the absolute value is small (3 kPa at best). Hence, it can be reasoned that the hot fluid does not lose a significant amount of pressure.

On the overall heat exchanger level, the mean HTCs for the hot and cold side are also reported, and are of the same order of magnitude. The simulation time is higher for the model by a factor of ten, since the number of slices used was conservatively large. The same simulation can be run in 30s with practically little to no loss in accuracy.

Based on the results of Tables 2, 3 and 5, it can be reasoned that the presented model is validated within the limits of the correlations used to predict the HTCs and friction factors.

7. CONCLUSIONS

A model for a brazed plate heat exchanger (BPHE) primarily acting as a condenser is presented and validated in this study. The HX can act as a condenser as part of a datacenter thermal management and heat recovery system. Conversely, the BPHE can also be used as an intermediate HX (regenerator) to enhance the enthalpy of the vapor leading to the compressor of the heat pump system. In this context, the BPHE will function in single-phase refrigerant-to-refrigerant heat exchanger.

The model presented in this study augments the work of Qiao et. al [5], but while the latter is general in nature, the current model is intended for only two fluids that can flow in only parallel or counter-flow configuration. The approach to solving a counter-flow configuration is also different, as is the model core solver (sequential for the current model versus parallel solve for [5]). Focus of the current model is accurate depiction of the condensation process, particularly for wet and dry-wall characteristics.

The modeling methodology is presented in detail for the fluid temperature distribution, channel wall temperatures and pressure drop across the exchanger. The results are validated against a commercial code, with a reported maximum difference in heat exchanger duty of 6.8% between the model and validation source.

Further work includes validating the model against experimental data to be collected from the system shown in Figure 2.

ACKNOWLEDGEMENTS

This material is based upon work supported by the NSF IUCRC Award No. IIP-1738782. Any opinions, findings, and conclusions or recommendations expressed in this paper are those of the authors and do not necessarily reflect the views of the National Science Foundation.

REFERENCES

[1] Y. Sverdlik, “Preempting Regulation, EU Operators Strike Green Data Center Pact,” *Data Center Knowledge*, Jan. 21, 2021. https://www.datacenterknowledge.com/energy/preempting-regulation-eu-operators-strike-green-data-center-pact (accessed May 04, 2021).

[2] H. Rong, H. Zhang, S. Xiao, C. Li, and C. Hu, “Optimizing energy consumption for data centers,” *Renew. Sustain. Energy Rev.*, vol. 58, pp. 674–691, May 2016, doi: 10.1016/j.rser.2015.12.283.

[3] R. L. Amalfi, J. B. Marcinichen, J. R. Thome, and F. Cataldo, “Design of Passive Two-Phase Thermosyphons for Server Cooling,” in *ASME 2019 International Technical Conference and Exhibition on Packaging and Integration of Electronic and Photonic Microsystems*, Anaheim, California, USA, Oct. 2019, p. V001T02A003. doi: 10.1115/IPACK2019-6386.

[4] R. Khalid, S. G. Schon, A. Ortega, and A. P. Wemhoff, “Waste Heat Recovery Using Coupled 2-Phase Cooling Heat-Pump Driven Absorption Refrigeration,” in *2019 18th IEEE Intersociety Conference on Thermal and Thermomechanical Phenomena in Electronic Systems (ITherm)*, May 2019, pp. 684–692. doi: 10.1109/ITHERM.2019.8757465.

[5] H. Qiao, V. Aute, H. Lee, K. Saleh, and R. Radermacher, “A new model for plate heat exchangers with generalized flow configurations and phase change,” *Int. J. Refrig.*, vol. 36, no. 2, pp. 622–632, Mar. 2013, doi: 10.1016/j.ijrefrig.2012.11.020.

[6] R. L. Amalfi and J. R. Thome, “Two-Phase Flow Simulations within Plate Heat Exchangers,” presented at the 17th Intersociety Conference on Thermal and Thermomechanical Phenomenon in Electronic Systems, ITHERM, United States, 2018.

[7] P. L. Kirillov and H. Ninokata, “Heat transfer in nuclear thermal hydraulics,” *Therm.-Hydraul. Water Cool. Nucl. React.*, pp. 357–492, Jan. 2017, doi: 10.1016/B978-0-08-100662-7.00007-5.

[8] R. Eldeeb, V. Aute, and R. Radermacher, “A Model for Performance Prediction of Brazed Plate Condensers with

 Copyright © 2021 by ASME

Conventional and Alternative Lower GWP Refrigerants," p. 11, 2014.
[9] R. K. Shah and D. P. Sekulić, *Fundamentals of heat exchanger design*. Hoboken, NJ: John Wiley & Sons, 2003.
[10] S. M. Zivi, "Estimation of steady-state steam void-fraction by means of the principle of minimum entropy generation," *J. Heat Transf.*, vol. 86, pp. 247–252, 1964.
[11] H. Kumar, "The Plate Heat Exchanger: Construction & Design," *Inst. Chem. Eng. Symp. Ser.*, vol. 2, no. 86, pp. 1275–1288, 1984.
[12] Z. H. Ayub, "Plate Heat Exchanger Literature Survey and New Heat Transfer and Pressure Drop Correlations for Refrigerant Evaporators," *Heat Transf. Eng.*, vol. 24, no. 5, pp. 3–16, Sep. 2003, doi: 10.1080/01457630304056.
[13] Y.-Y. Yan, H.-C. Lio, and T.-F. Lin, "Condensation heat transfer and pressure drop of refrigerant R-134a in a plate heat exchanger," *Int. J. Heat Mass Transf.*, vol. 42, no. 6, pp. 993–1006, Mar. 1999, doi: 10.1016/S0017-9310(98)00217-8.
[14] J. Zhang, M. R. Kærn, T. Ommen, B. Elmegaard, and F. Haglind, "Condensation heat transfer and pressure drop characteristics of R134a, R1234ze(E), R245fa and R1233zd(E) in a plate heat exchanger," *Int. J. Heat Mass Transf.*, vol. 128, pp. 136–149, Jan. 2019, doi: 10.1016/j.ijheatmasstransfer.2018.08.124.
[15] F. Vakili-Farahani, R. L. Amalfi, and J. R. Thome, "Two-Phase Heat Transfer and Pressure Drop within Plate Heat Exchangers," *Encyclopedia of Two-Phase Heat Transfer and Flow II*. pp. 145–215, 2015.
[16] J. Huang, T. J. Sheer, and M. Bailey-McEwan, "Heat transfer and pressure drop in plate heat exchanger refrigerant evaporators," *Int. J. Refrig.*, vol. 35, no. 2, pp. 325–335, Mar. 2012, doi: 10.1016/j.ijrefrig.2011.11.002.

Copyright © 2021 by ASME